nature

https://doi.org/10.1038/s41586-020-2321-x

Supplementary information

Coherent interaction between free electrons and a photonic cavity

In the format provided by the authors and unedited

Kangpeng Wang, Raphael Dahan, Michael Shentcis, Yaron Kauffmann, Adi Ben Hayun, Ori Reinhardt, Shai Tsesses & Ido Kaminer✉

Supplementary Information

Coherent interaction between free electrons and a photonic cavity

*Kangpeng Wang[1], Raphael Dahan[1], Michael Shentcis[1], Yaron Kauffmann[2], Adi Ben Hayun[1], Ori Reinhardt[1], Shai Tsesses[1], and Ido Kaminer[1]**

1. Solid State Institute and Faculty of Electrical Engineering, Technion – Israel Institute of Technology, Haifa 32000, Israel
2. Department of Materials Science & Engineering, Technion – Israel Institute of Technology, Haifa 32000, Israel

* kaminer@technion.ac.il

Table of Contents

Supplementary Note 1 – Quantum theory of electron–cavity-photon interaction

In the following section, we will present a complete quantum theory of a free electron interacting with a photonic cavity mode, in which both the electron and the cavity mode are quantized. The electron is described by a quantum wavefunction and the cavity mode is described by second quantization. We show how to get the conventional photon-induced near-field electron microscopy (PINEM)[1] expression from the complete quantum theory. We further extend the theory to a time-dependent interaction of an electron pulse with a time-dependent cavity photon population trapped in a resonant photonic structure. Our theory is based on the classical-field formalism[2–4] and its quantum generalization developed in very recent works[5,6]. Using this theory, we analyze for the first time the full scenario of a general quantum electron interacting with a general cavity state.

We begin from writing a Schrodinger equation for the electron. The interaction Hamiltonian can be written as $H_{\mathrm{int}} = (e/m)\,\vec{p}\cdot\vec{A}$ with a vector potential whose z component is connected to the electric field phasor as $A_{\mathrm{z}}(\mathrm{t}) = E_z(z)(2/\omega)\sin(\omega t)$. Under the slowly-varying envelope approximation, we can multiply the above by additional terms to account for two phenomena: (1) The finite lifetime of the cavity; (2) The finite temporal laser pulse. These can be described by the common frequency dependence of (1) a Lorentzian $\frac{1/\tau^2}{(\Omega-\omega)^2+1/\tau^2}$ using Ω as the frequency dependence and τ as the cavity lifetime, and (2) a Gaussian $e^{-\frac{1}{2}\sigma_L^2(\Omega-\omega)^2}$ with σ_L as the temporal laser pulse width. These two terms are multiplied in the frequency domain, resulting in an additional time-domain convolution term of $A_{\mathrm{z}}(\mathrm{t}) = E_z(z)(2/\omega)\sin(\omega t)\left[e^{-t^2/\sigma_L^2} * u(t)\right]$ with $u(t)$ the Fourier transform of the Lorentzian.

The interaction Hamiltonian in terms of creation and annihilation operators for the

electron[12] and the field[26] can be written as:

$$H_{int} = \frac{2\hbar v}{L}\left(g_{Qu}^{*} b^{\dagger} a + g_{Qu} b a^{\dagger}\right)\sin(\omega t), \qquad (S1)$$

where L is the characteristic length, v is the electron's velocity, and ω is the photon frequency. The parameter g_{Qu} is the quantum coupling strength (generalizing ref[5]), the quantum equivalent of the dimensionless coupling strength of the conventional PINEM formalism[2,3] β. By taking into consideration the slowly varying envelope and assuming a short interaction length, we get:

$$g_{Qu}(t) = \frac{1}{|\alpha|}\beta\left[e^{-t^2/\sigma_L^2} * u(t)\right] = \frac{1}{|\alpha|}\frac{e}{\hbar\omega}\left[e^{-t^2/\sigma_L^2} * u(t)\right]\int E_z(z) e^{-i\frac{\omega}{v}z} dz, \qquad (S2)$$

where we associate the electric field to a coherent photonic state $|\alpha\rangle$, i.e., a Fock-state superposition with the following Poisson distribution:

$$|\alpha\rangle = \sum_{n=0}^{\infty} e^{-\frac{1}{2}|\alpha|^2} \frac{\alpha^n}{\sqrt{n!}} |n\rangle \ . \qquad (S3)$$

The cavity field's creation and annihilation operators a, and the electron raising and lowering operators b obey the following relations:

$$\begin{aligned} b|E_k, n\rangle &= |E_{k-1}, n\rangle \\ b^{\dagger}|E_k, n\rangle &= |E_{k+1}, n\rangle \\ a|E_k, n\rangle &= \sqrt{n}|E_k, n-1\rangle \\ a^{\dagger}|E_k, n\rangle &= \sqrt{n+1}|E_k, n+1\rangle \end{aligned} \ , \qquad (S4)$$

where $|E_k\rangle$ represents an electron of energy $E_0 + k\hbar\omega_0$, for some arbitrarily chosen baseline energy E_0; $|n\rangle$ represents the photonic Fock state of index n and $|E_k, n\rangle = |E_k\rangle \otimes |n\rangle$.

The full scattering matrix is

$$\hat{S}(t) = \mathcal{T} \exp\left[-\frac{i}{\hbar}\int_{-\infty}^{t} \xi(b a^{\dagger} + b^{\dagger} a) dt'\right], \qquad (S5)$$

where $\xi(t')$ is the slowly-varying coupling strength with units of energy, and $\mathcal{T}$ is

the time-ordering operator. The slow envelope approximation allows us to define $b(t') = be^{-i\omega t'}$ and $a(t') = ae^{-i\omega t'}$ and to pull their operator products $ba^\dagger$ and $b^\dagger a$ out of the integral. This separation allows us to remove the time-ordering operator and get $\hat{S} = e^{g_{Qu}ba^\dagger - g_{Qu}^* b^\dagger a}$, where g_{Qu} holds the slowly-varying time-dependence, while letting us work algebraically with the non time-dependent a and b. We can now use this scattering matrix to evaluate the transition probabilities $P_{k',n'\to k,n} = \left|\langle E_k, n|\hat{S}|E_{k'}, n'\rangle\right|^2$.

To describe the most general electron–cavity photon state, we employ a density matrix description. We start from the general electron–cavity photon pure state that is an arbitrary superposition of the $|E_k, n\rangle$ states, defined by a set of coefficients $c_{k,n}^{(i)}$:

$$|\psi_i\rangle = \sum_{\substack{k=-\infty,\\ n=0}}^{\infty} c_{k,n}^{(i)} |E_k, n\rangle . \qquad (S6)$$

Using the Zassenhaus formula, we can expand the $\hat{S}$ matrix and write it as

$$\hat{S} = e^{\frac{|g_{Qu}|^2}{2}} \sum_{m,l=0}^{\infty} \frac{\left(-g_{Qu}^*\right)^m g_{Qu}^l}{m!\, l!} (b^\dagger a)^m (ba^\dagger)^l. \qquad (S7)$$

The state of the system described in Eq. S6 is a pure state and therefore its density matrix is simply given as $\rho^{(i)} = |\psi_i\rangle\langle\psi_i|$, which results in the matrix elements $\rho_{k,n,k',n'}^{(i)} = c_{k,n}^{(i)} \left(c_{k',n'}^{(i)}\right)^*$. Now, to retrieve the transition probabilities, we can use the creation and annihilation operators and calculate the $\hat{S}$ matrix elements

$$\hat{S}_{k,n,k',n'} = \langle E_k, n|\hat{S}|E_{k'}, n'\rangle$$
$$= e^{\frac{|g_{Qu}|^2}{2}} g_{Qu}{}^{|n'-n|} \sum_{l=0}^{\infty} \frac{\left(-\left|g_{Qu}\right|^2\right)^l (n + l + \max\{0, n' - n\})!}{l!\,(l + |n' - n|)!\sqrt{n'!\, n!}} \delta_{k+n=k'+n'} . \qquad (S8)$$

The final state $|\psi_f\rangle$ is the result of the scattering matrix $\hat{S}$ acting on $|\psi_i\rangle$. This means that we can write the density matrix for the final state $\rho^{(f)}$ by:

$$\rho^{(f)} = \left|\psi_f\right\rangle\left\langle\psi_f\right| = \hat{S}|\psi_i\rangle\langle\psi_i|\hat{S}^\dagger = \hat{S}\rho^{(i)}\hat{S}^\dagger . \tag{S9}$$

This expression is correct for any general density matrix for the initial state $\rho^{(i)}$. Solving for the final density matrix $\rho^{(f)}$ we can formulate the following expression:

$$\begin{aligned}&\rho^{(f)}_{k,n,\,k',n'} = \\ &= \left[\sum_{x=-\infty}^{k+n}\left[e^{\frac{|g_{Qu}|^2}{2}}\cdot g_{Qu}^{|k-x|}\sum_{l=0}^{\infty}\frac{\left(-\left|g_{Qu}\right|^2\right)^l(n+l+\max(0,k-x))!}{l!\,(l+|k-x|)!\sqrt{n!\,(k+n-x)!}}c^{(i)}_{x,k+n-x}\right]\right]\cdot \\ &\cdot\left[\sum_{x=-\infty}^{k'+n'}\left[e^{\frac{|g_{Qu}|^2}{2}}g_{Qu}^{|k'-x|}\sum_{l=0}^{\infty}\frac{\left(-\left|g_{Qu}\right|^2\right)^l(n'+l+\max(0,k'-x))!}{l!\,(l+|k'-x|)!\sqrt{n'!\,(k'+n'-x))!}}c^{(i)}_{x,k'+n'-x}\right]\right]^* .\end{aligned} \tag{S10}$$

The density matrix allows us to find the electron–cavity photon probabilities $P_{k,n} = \rho_{k,n,k,n}$ and we get:

$$\begin{aligned}&P_{k,n} = \left|c^{(f)}_{k,n}\right|^2 = \\ &= e^{|g_{Qu}|^2}\left|\sum_{l=0}^{\infty}\frac{\left(-\left|g_{Qu}\right|^2\right)^l}{l!}\sum_{x=-\infty}^{k+n}\frac{g_{Qu}^{|k-x|}(n+l+\max\{0,k-x\})!\,c^{(i)}_{x,k+n-x}}{(l+|k-x|)!\sqrt{n!\,(k+n-x)!}}\right|^2\end{aligned} \tag{S11}$$

So far, we left all derivations as general as possible, solving for any initial electron state and any initial photon cavity state (or their combination $\rho^{(i)}$). We now want to retrieve the simple case of a PINEM interaction and obtain the known PINEM probabilities for our scenario. We will begin by picking a specific initial electron–cavity-photon state: a baseline energy electron and a cavity of a coherent state $|\alpha\rangle$, as defined in Eq. S3, resulting in:

$$c^{(i)}_{k,n} = e^{-\frac{|\alpha|^2}{2}}\frac{\alpha^n}{\sqrt{n!}}\delta_{k,0} . \tag{S12}$$

Plugging this initial state into Eq. S11, and noting the time dependence of g_{Qu}, we get:

$$P_{k,n} = \begin{cases} \left| e^{\frac{|g_{Qu}|^2-|\alpha|^2}{2}} \frac{{g_{Qu}}^{|k|}\alpha^{k+n}}{\sqrt{n!}} \sum_{l=0}^{\infty} \frac{\left(-|g_{Qu}|^2\right)^l}{l!\,(|k|+l)!} \frac{(n+l+\max\{0,k\})!}{(k+n)!} \right|^2, & k+n \geq 0 \\ 0, & k+n < 0 \end{cases} \quad (S13)$$

Next, we focus on the case of $|g_{Qu}| \ll 1$, which means that the quantum coupling strength is weak (note that the conventional PINEM field β can still be very strong, e.g., $\gg 1$). The result of $|g_{Qu}| \ll 1$ is that the discrete electron energy change is much smaller than the number of photons in the field ($|k| \ll n$). Therefore, we may neglect k (in its various forms) wherever it is summed with n. Focusing on the summation term, and using the definition $\beta\left[e^{-t^2/\sigma_L^2} * u(t)\right] = g_{Qu}|\alpha| \approx g_{Qu}\sqrt{n}$ and Stirling's formula, we can simplify Eq. S13:

$$\frac{\left(-|g_{Qu}|^2\right)^l}{l!\,(|k|+l)!} \frac{(n+l+\max\{0,k\})!}{(k+n)!} \approx \frac{\left(-|g_{Qu}|^2\right)^l}{l!\,(|k|+l)!} \frac{(n+l)!}{n!} \approx \frac{\left(-|g_{Qu}|^2\right)^l}{l!\,(|k|+l)!} n^l \approx \frac{\left(-\left|\beta\left[e^{-t^2/\sigma_L^2} * u(t)\right]\right|^2\right)^l}{l!\,(|k|+l)!}, \quad (S14)$$

which results in

$$P_{k,n} = e^{|g_{Qu}|^2-|\alpha|^2} \left| \frac{{g_{Qu}}^{|k|}\alpha^n}{\sqrt{n!}} \sum_{l=0}^{\infty} \frac{\left(-\left|\beta\left[e^{-t^2/\sigma_L^2} * u(t)\right]\right|^2\right)^l}{l!\,(|k|+l)!} \right|^2. \quad (S15)$$

The magnitude of g_{Qu} is approximately:

$$\left|g_{Qu}^{|k|}\right| \approx \left| \frac{2|\beta[e^{-\frac{t^2}{\sigma_L^2}} * u(t)]}{2\alpha} \right|^{|k|}. \quad (S16)$$

Since we have $\left|g_{Qu}\right| \ll 1$, then $e^{|g_{Qu}|^2} \approx 1$. Substituting Eq. S16 into Eq. S15, and using the above approximation, we finally get:

$$P_{k,n} = J_{|k|}^2\left(2|\beta|\left[e^{-t^2/\sigma_L^2} * u(t)\right]\right)\left|e^{-\frac{1}{2}|\alpha|^2}\frac{\alpha^n}{\sqrt{n!}}\right|^2 \quad . \qquad (S17)$$

We notice that in fact the electron and photon states are now separable, and we can extract the electron probabilities, corresponding to the known PINEM expression[10-12], $P_k = J_{|k|}^2\left(2|\beta|\left[e^{-t^2/\sigma_L^2} * u(t)\right]\right)$, but also accounting for the finite cavity lifetime and finite electron pulse width. The function $u(t)$ can be calculated as the Fourier transform of a Lorenzian $u(t) = \Theta(t)e^{-t/\tau}/\tau$, describing an exponential decay following the lifetime τ of the photonic mode, where $\Theta(t)$ is the Heaviside step function. The electron probability to be at an energy state k is therefore

$$P_k = J_k^2\left(2|\beta|e^{-t^2/\sigma_L^2} * (\Theta(t)e^{-t/\tau}/\tau)\right), \qquad (S18)$$

which has the same Bessel function argument as in the main text. The next section explains this formula as a direct extension of the conventional PINEM theory, and describes the additional effect of the electron pulse duration – achieving Eq. 1 from the main text.

Supplementary Note 2 – Full time dependence of the electron probabilities in PINEM

This section derives the central equation of the main text, which captures all the effects we observed (PINEM energy peaks used for nearfield imaging, time-dependent spectra used for lifetime measurements, and Rabi oscillations used in spatial scanning):

$$P_k(E,t) = J_k^2\left(2|\beta|(\Theta(t)e^{-\frac{t}{\tau}}/\tau) * e^{-(t/\sigma_L)^2}\right) * G(t-\zeta E,\sigma_e), \qquad (1)$$

where the standard deviations σ_e, σ_L of the electron and the laser pulses depend on their durations τ_e, τ_L via $\sigma_{e,L} = \tau_{e,L}/(2\sqrt{\ln 2})$.

Generally, we can start by describing the electron energy spectra in PINEM experiments as $P(E,t) = \sum_{k=-\infty}^{+\infty} f_0(E-k\hbar\omega)P_k(E-k\hbar\omega,t)$, where f_0 is the initial electron probability density in the electron energy E. Experimental conditions dictate uncertainty of the initial electron energy, which is known as the zero-loss peak (ZLP) width.

Before considering the effect of the lifetime of a photonic cavity, we consider the effects of the time durations of the electron pulse and the laser pulse (which will correspond to the formalism reported in the literature[2,3,7]). We assume that the initial electron energy probability density has a Gaussian-like profile $f_0 = G(E,\sigma_E)$, where the Gaussian function G is defined as $G(x,\sigma) = \frac{1}{\sigma\sqrt{\pi}}e^{-(x/\sigma)^2}$ and the standard deviation σ_E depends on full-width half maximum (FWHM) width of the ZLP w_E via $\sigma_{\mathrm{E}} = w_E/(2\sqrt{\ln 2})$. Thus, we have the electron energy spectra (probability density) in PINEM experiments by $P(E,t) = \sum_{k=-\infty}^{+\infty} G(E-k\hbar\omega,\sigma_E)P_k(E-k\hbar\omega,t)$.

The electron pulses are often chirped, because the high energy electrons travel faster than the low energy ones[8]. Using the definition of the electron's intrinsic chirp coefficient ζ, we can add an additional energy dependence

$$P(E,t) = \sum_{k=-\infty}^{+\infty} G(E-k\hbar\omega,\sigma_E)P_k(E-k\hbar\omega,t) * G(t-\zeta E,\sigma_e), \qquad S(19)$$

where the convolution (denoted by *) accounts for the influence of the temporal electron pulse $G(t,\sigma_e)$.

1. The electron probabilities in PINEM without a cavity effect

For electron and laser pulses with (temporal) Gaussian envelopes that interact according to the conventional PINEM theory, i.e., no cavity involved, we can write $P_k(t) = J_k^2\left(2|\beta|e^{-t^2/\sigma_L^2}\right) * G(t,\sigma_e)$, where e^{-t^2/σ_L^2} is the time dependence of the excitation field[7]. The PINEM probability density from Eq. S19 is accordingly:

$$P(E,t) = \sum_{k=-\infty}^{+\infty} G(E-k\cdot\hbar\omega,\sigma_E)\, J_k^2\left(2|\beta|e^{-t^2/\sigma_L^2}\right) * G(t-\zeta(E-k\cdot\hbar\omega),\sigma_e)\,. \quad (S20)$$

This probability density corresponds to Eq. 1 from the main text, except for the contribution of the cavity.

Note that the t-dependence on the right-hand side of Eq. S20 is the result of the temporal convolution between the pulses, and takes the role of the delay between the electron and laser pulses. Eq. S20 can be equivalently written as:

$$P(E,t) = \frac{1}{\pi\sigma_E\sigma_e}\sum_{k=-\infty}^{+\infty} e^{-\frac{(E-k\cdot\hbar\omega)^2}{\sigma_E^2}} \int_{-\infty}^{+\infty} J_k^2\left(2|\beta|e^{-\frac{t'^2}{\sigma_L^2}}\right) e^{-\frac{[t-t'+\zeta(E-k\cdot\hbar\omega)]^2}{\sigma_e^2}} dt'\,. \quad (S21)$$

Eq. S21 corresponds to the formalism reported in the literature[2,3,7].

2. The electron probabilities in PINEM with the cavity effect

To include the effect of the photonic cavity, which enhances the interaction and extends its duration by a lifetime τ, we take the full form of Eq. S18, $P_k = J_k^2\left(2|\beta|e^{-t^2/\sigma_L^2} * \Theta(t)e^{-t/\tau}/\tau\right)$. This expression can be understood as the convolution of the laser pulse with the cavity's impulse response function $u(t) = \Theta(t)e^{-t/\tau}/\tau$. This impulse response also appears in optical pump-probe theory[9]. Altogether, both approaches, with a classical or a quantum photonic field, correspond to Eq. 1 in the main text.

We obtain the energy probability density for cavity photons as a function of the pump-probe delay t:

$$P(E,t) = \sum_{k=-\infty}^{+\infty} G(E - k\cdot\hbar\omega, \sigma_{\mathrm{E}})\, J_k^2\left(2|\beta|u(t) * e^{-t^2/\sigma_L^2}\right) * G(t - \zeta(\mathrm{E} - k\cdot\hbar\omega), \sigma_e), \quad (S22)$$

or

$$P(E,t) = \frac{1}{\pi\sigma_E\sigma_e}\sum_{k=-\infty}^{+\infty} e^{-\frac{(E-k\cdot\hbar\omega)^2}{\sigma_E^2}} \int_{-\infty}^{+\infty} e^{-\frac{[t'-t-\zeta(E-k\cdot\hbar\omega)]^2}{\sigma_e^2}} \cdot J_k^2\left(\sqrt{\pi}|\beta_0| e^{\left(\frac{\sigma_L^2}{4\tau^2}-\frac{t'}{\tau}\right)} \mathrm{erfc}\left(\frac{t'}{\sigma_L} - \frac{\sigma_L}{2\tau}\right)\right) dt'. \quad (S23)$$

Note that as the lifetime shortens $(\tau \to 0)$, we will have $u(t) \to \delta(\mathrm{t})$, where $\delta(t)$ is the Dirac Delta function. Then $u(t) * |\beta(t)| = |\beta(t)|$ and Eq. S22 and S23 converge to S20 and S21 respectively.

Supplementary Note 3 – Data processing: extracting the lifetime and the PINEM field from the energy spectrum of the electron probe

This section presents the analysis we perform for extracting the lifetime from the electron–cavity-photon interaction. We also present the conversion from the measured probabilities (histogram) of the electron energy spectrum to the PINEM coupling strength, and discuss the conversion from the PINEM coupling strength to the electric field.

These parameters can be extracted in several different strategies. In case one is interested in maintaining high spatial resolution, measuring the lifetime and field strength at each point, we can use a focused electron beam as in scanning transmission electron microscopy (STEM) and perform the measurement point-by-point (as done in Fig. 3c). Alternatively, in regular transmission using a wide electron beam (TEM mode), we can use energy filtered images to extract simultaneous information at different points in space (as done in Figs. 2c, 3b and 4).

For the measurement of the lifetime, we can use the fact that the entire photonic mode decays together to combine the information from different points in space and analyze the combined electron energy spectrum. In this case, the interaction probability density is found to be well-described by an integral over the lateral *x*-*y* plane, which is perpendicular to the electron propagation direction *z*

$$P(E,t) = \iint P\big(E,t,\beta_0(x,y)\big)dxdy\,. \qquad (S24)$$

In the case of a photonic crystal, the integration area in Eq. S24 can be considered to be a single unit-cell (since the transverse interaction area is much larger than a single cell). We find that in practice the EELS of the Bloch modes can be well-fitted empirically using the expression $P(E,t) = \int_0^D P(E,t,\beta_0 e^{-x})dx$, which contains a single dimensionless parameter D. Substituting the β_0 by $\beta_0 e^{-x}$ in Eq. S23 and introducing an additional integral, we have the probability density of the EELS in a photonic crystal:

$$P(E,t)=\frac{1}{\pi\sigma_E\sigma_e}\sum_{k=-\infty}^{+\infty}e^{-\frac{(E-k\cdot\hbar\omega)^2}{\sigma_E^2}}\int_{-\infty}^{+\infty}\int_{0}^{D}e^{-\frac{[t'-t-\zeta(E-k\cdot E_L)]^2}{\sigma_e^2}}$$

$$\cdot J_k^2\left(\sqrt{\pi}|\beta_0 e^{-x}|e^{\left(\frac{\sigma_L^2}{4\tau^2}-\frac{t'}{\tau}\right)}\operatorname{erfc}\left(\frac{t'}{\sigma_L}-\frac{\sigma_L}{2\tau}\right)\right)dx\,dt'. \quad (S25)$$

To obtain the lifetime τ from our experiments, we developed an optimization algorithm to minimize the difference between the experimental data P_{exp} (e.g., Fig. 4a) and the theoretical one in Eq. S25. We define the following quadratic error function F:

$$\text{Minimize } F(\sigma_E,\sigma_e,\beta_0,\sigma_L,\tau,\zeta,D)=\left|P_{\text{exp}}-P_{\text{Eq. S25}}\right|^2. \quad (S26)$$

The optimization algorithm can run over all the parameters defined above: $\sigma_E,\sigma_e,\beta_0,\sigma_L,\tau,\zeta$, and D, search for the optimum by an interior-point method. First, we evaluate F using an initial guess of all the parameters. Then a series of changes are applied iteratively to the parameters (as in gradient descent algorithms), each time checking that we obtain a new F. The iterations stop when a minimum of F is obtained and optimal parameters $\sigma_E,\sigma_e,\beta_0,\sigma_L,\tau,\zeta$, and D are found. While such an algorithm often produces a local minimum and not the global one, we have not experienced this problem in practical cases for the calculation of the lifetime (Fig. 4) or Rabi phase (Fig. 3). Testing different initial conditions consistently resulted in the same optimal fit of the parameters. We believe that such convenient optimization conditions occur whenever using relatively weak interactions (β not much larger than 1), and also when using electron pulse durations that are longer than the laser pulse duration (so the average interaction is weakened).

We used the above procedure with a wide electron beam to find τ in Fig. 4. We also get the PINEM field β (averaged over the unit cell). When using a focused electron beam we get β at each point, as we have done in Fig. 3, and thus we can obtain the nearfield map in a STEM mode. From the PINEM field β, it is possible to get the electric field at each point in *x*-*y*, integrated along the z axis. Finding the entire electric field in 3D would also be possible by tilting the sample and incident laser relative to the electron, thus achieving full-field tomography in 3D.

There is another strategy for extracting the nearfield map, which we use in Fig. 2.

Using a wide electron beam and filtering it by energy (blue frame in Extended Data Fig. 1a) we obtain the entire map simultaneously. This map contains integrated electron probabilities, from which the conversion to the PINEM field is not trivial. In some cases, the conversion is not monotonic, and then some prior knowledge about the field distribution is required in order to translate the measurement to the actual field[1,2]. However, when using a weak field (e.g., as for sensitive samples), then this conversion could be monotonic. Similarly, when the electron pulse duration is longer than the laser pulse duration we could expect that the conversion may also be monotonic.

Supplementary Note 4 – Fit of the spatial-analogue Rabi oscillations

Here we present the method used to obtain the Rabi phases defined by $2|\beta|$ from the EELS map (Fig. 3c) and spectra (Fig. 3e) using Eq. 1, in which the electron is quantum and the field is classical (also see Supplementary Note 1 and 2). We also explain the comparison with the classical theory.

First, we took the electron energy spectrum at each x position (Supplementary Fig. 1a) and normalize it to total probability of 1. Since the lifetime is smaller than the pulse durations, it is neglected for the fits and results in this case. The fitted map is shown in Supplementary Fig. 1b.

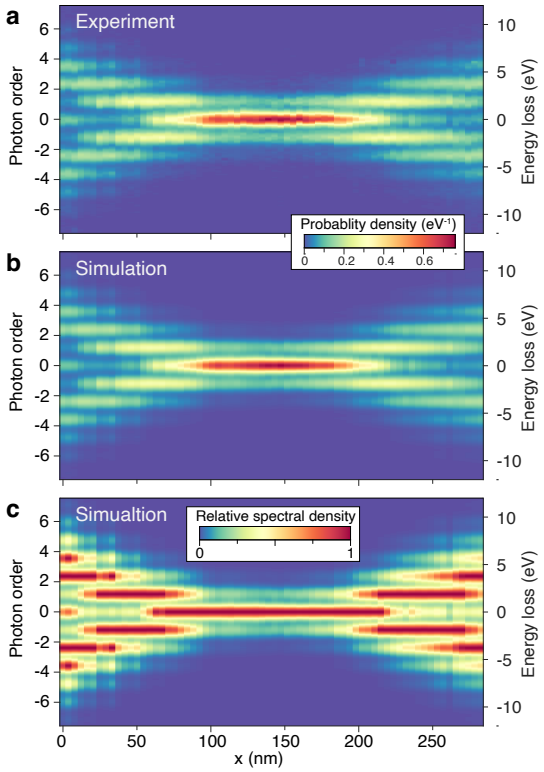

Supplementary Fig. 1 | Electron energy spectrum recorded as a function of electron probe position. a, Measured electron energy map. This map is from the same data in Fig. 3c but here its integrated probability for each *x* position normalized to 1. **b,** Simulated electron energy map from the fit of Eq. 1. **c**, Simulated electron energy map in **b** after normalizing to its maxima, better showing the oscillation of the peaks, as in literature[4] and Fig. 3c.

We also fitted the measured electron energy map to a classical theory[10], which assumes a point electron of mass m and charge q moving under the relativistic Newton Lorentz force. In our case, the electron energy change (gain or loss) can be found as an integral over the electric field that resembles the PINEM field: $\Delta E = 2e\int dz\, \mathcal{E}_z(z)e^{-i\omega z/v}$. When we assume that the electron arrival time is random relative to the phase of the field, we find that the electron after the interaction is described by the following probability density for the electron's energy change E:

$$p_{classical}(E) = \frac{1}{\pi\Delta E\sqrt{1-\frac{E^2}{\Delta E^2}}}\,, \qquad (S27)$$

Using the same initial Gaussian energy distribution (the zero-loss peak) as in Eq. 1, we perform a convolution on Eq. S27 to obtain the classical fit (dashed curves) in Fig. 3e

$$P_{classical}(E) = p_{classical}(E) * G(E,\sigma_E)\,. \qquad (S28)$$

The definition of Gaussian function $G(E,\sigma_E)$ and the relationship σ_E to the electron's zero-loss peak width can be found in the Supplementary Note 2.

Supplementary Note 5 – Subtraction of the zero-loss peak spectrum

In Fig. 4b of the main text, we presented the probability density of the electron–cavity-photon interaction at each delay time, which is the result of subtracting the spectrum of the non-interacting electron (i.e., the zero-loss peak, ZLP)[8,4]. This subtraction is valid because the PINEM interaction moves the electrons of the ZLP to both sides, and we can quantify this interaction by subtraction of the non-interacting spectrum. After the subtraction, the spectrum at the zero-loss peak becomes negative (since the interacting electrons are subtracted from the zero-loss peak energies and move to the gain and the loss sides). There are three advantages for using the ZLP subtracted spectra to get the probability of electron–cavity-photon interaction (the ratio of electrons that interacted with the photons out of all electrons as in Fig. 4c):

(1) We can precisely separate the interacting electrons from the non-interacting ones. This method is especially useful when the ZLP and first order peaks partially overlap, and are thus hard to separate in other ways.

(2) The subtraction improves the signal-to-noise and thus provides higher stability for the quantitative fit we perform. This method is especially important for weak interaction strengths or very low laser intensities for which the signal in the side-lobes is small compared to the high ZLP.

(3) The background noise and additional loss mechanisms in the spectrum (e.g., plasmon peak) can be greatly reduced.

Supplementary Note 6 – Photonic crystal Q-factor calculation

The photonic crystal membrane contains extended cavity modes, with properties such as the quality-(Q-)factor, as in localized photonic cavities. The Q factor of the photonic crystal cavity modes can be calculated through the bandwidth of the resonance

$$Q = \frac{f_0}{\Delta f},$$

where $f_0 = c/\lambda$ is the resonant frequency, and Δf is the full-width half maximum (FWHM) of the resonance bandwidth. From the FDTD simulation of the photonic crystal bandstructure (Extended Data Fig. 2a), we obtained the spectral response of the photonic crystal as shown in Supplementary Fig. 2. The high-Q mode (upper panel of Fig. 4a) was found at 835 nm wavelength and 4.4° incident angle in the measurements. In the simulated bandstructure (Extended Data Fig. 2a), the same mode was found at 364.3 THz frequency (823 nm) and 4.4° incident angle. The FWHM bandwidth Δf of this high-Q mode in the simulation, is determined to be 1.02 THz. The Q-factor obtained from the simulations is ~357, showing a good match to the value obtained through the lifetime measurement with the electron probe (~384, presented in the main text).

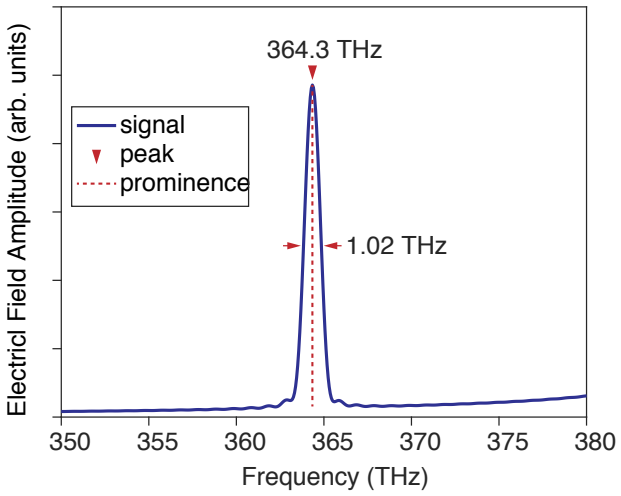

Supplementary Fig. 2 | Estimating the quality-(Q-) factor of the high-Q mode (upper panel of Fig. 4a) using the simulated bandstructure (Extended Data Fig. 2a). The Q-factor corresponds well to the result achieved from measurement (in the main text).

Supplementary Note 7 – Laser spot diameter

In order to estimate the laser spot diameter on the sample located in the TEM column, we used a camera placed on the focal plane of the parabolic mirror used for focusing light on the sample (Supplementary Fig. 3a). The image of the pump laser (730 nm wavelength) spot is captured in Supplementary Fig. 3b. To obtain the laser spot size, a Gaussian model, $G(x,y) = A \cdot \exp\left(-(x^2+y^2)/\sigma^2\right)$, is used to fit this image by a nonlinear regression algorithm. The full width half maximum diameter, D, was determined to be 69.0 µm via the relationship $D = 2\sqrt{\ln 2}\sigma$ and presented as red circle in Supplementary Fig. 3b.

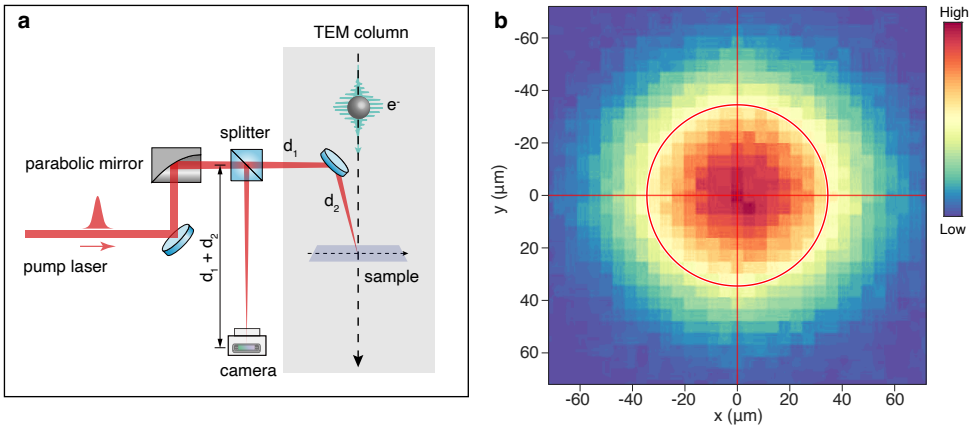

Supplementary Fig. 3 | Measurement of spatial spot size of the laser pulse. a, Scheme of the laser spot size measurement. A parabolic mirror is used to focus the laser on the sample surface. The distance from the sample to the beam splitter is $d_1 + d_2$. To measure the laser spot size on the sample surface, a calibrated camera is placed at the same distance $d_1 + d_2$ from the beam splitter. **b,** The laser (730 nm wavelength) spot image, as captured by the camera. Solid lines mark the laser spot center. The circle presents the fitted spot diameter (69.0 µm) from the Gaussian model as explained above.

Supplementary References

1. Barwick, B., Flannigan, D. J. & Zewail, A. H. Photon-induced near-field electron microscopy. *Nature* **462**, 902 (2009).
2. García de Abajo, F. J., Asenjo-Garcia, A. & Kociak, M. Multiphoton absorption and emission by interaction of swift electrons with evanescent light fields. *Nano Lett.* **10**, 1859 (2010).
3. Park, S. T., Lin, M. & Zewail, A. H. Photon-induced near-field electron microscopy (PINEM) theoretical and experimental. *New J. Phys.* **12**, 123028 (2010).
4. Feist, A. *et al.* Quantum coherent optical phase modulation in an ultrafast transmission electron microscope. *Nature* **521**, 200 (2015).
5. Kfir, O. Entanglements of electrons and cavity-photons in the strong coupling regime. *Phys. Rev. Lett.* **123**, 103602 (2019).
6. Di Giulio, V., Kociak, M. & García de Abajo, F. J. Probing Quantum Optical Excitations with Fast Electrons. *Optica **6**,* 1524–1534 (2019).
7. Vanacore, G. M. *et al.* Attosecond coherent control of free-electron wave functions using semi-infinite light fields. *Nat. Comm.s* **9**, 2694 (2018).
8. Park, S. T., Kwon, O.-H. & Zewail, A. H. Chirped imaging pulses in four-dimensional electron microscopy: femtosecond pulsed hole burning. *New J. Phys.* **14**, 053046 (2012).
9. Prasankumar, R. P. & Taylor, A. J. *Optical techniques for solid-state materials characterization*. (CRC Press, 2016).
10. Nehemia, S. *et al.* Observation of the Stimulated Quantum Cherenkov Effect. *arXiv* 1909.00757 (2019).